Simulation of the Second Harmonic Ultrasound Field in Heterogeneous Soft Tissue Using a Mixed Domain Method

Juanjuan Gu and Yun Jing, *Senior Member, IEEE*

Abstract— A mixed-domain method dubbed frequency-specific mixed domain method is introduced for the simulation of the second harmonic ultrasound field in weakly heterogeneous media. The governing equation for the second harmonics is derived based on the quasilinear theory. The speed of sound, nonlinear coefficient, and attenuation coefficient are all spatially varying functions in the equation. The fundamental frequency pressure field is first solved by the frequency-specific mixed domain method, and it is subsequently used as the source term for the second harmonics equation. This equation can be again solved by the frequency-specific mixed domain method to rapidly obtain the second harmonic pressure field. Five two-dimensional cases, including one with a realistic human tissue map, are studied to systematically verify the proposed method. Results from the previously developed transient mixed domain method are used as the benchmark solutions. Comparisons show that the two methods give similar results for all cases. More importantly, the frequency-specific mixed domain method has a crucial advantage over the transient mixed domain method in that it can be two orders of magnitude faster.

***Index Terms*—Focused ultrasound, heterogeneous media, second harmonics, frequency-specific mixed domain method (FSMDM), one-way propagation.**

I. Introduction

Nonlinear ultrasound, a branch of nonlinear acoustics, is of great importance in biomedical ultrasound for both diagnostic and therapeutic applications [1]. For instance, the presence of acoustic nonlinearity could improve B-mode imaging because the harmonic beams are narrower and they have lower sidelobes than those of the fundamental frequency [2]. The combination of the fundamental frequency and its harmonics can enhance the image quality and help better visualize tissue structures [3]. Nonlinear parameter diffraction-based tomography can help better distinguish diseased tissues from healthy ones compared to ultrasound imaging purely based on linear parameters [4], [5]. On the other hand, when high intensity focused ultrasound (HIFU) is used for therapeutic applications, the nonlinear effect can be pronounced, though its extent very much depends on factors such as *F*-number [6], frequency, propagation medium [7], and sonication protocol (whether it is for hyperthermia [8], [9], [10], thermal ablation [11], inertial cavitation [11], [12], or boiling [13]).

Numerical modeling is vital for facilitating the applications of nonlinear ultrasound. A number of numerical methods have been developed to model nonlinear ultrasound propagation [14], [15], [16], [17]. Some of the solvers assume that the propagating medium is homogeneous [16], [17], [18]. Though it is argued that such an assumption is reasonable for soft tissues, more accurate results can be obtained if tissue heterogeneities are taken into account. This is especially important when studying phase aberration in biological tissue [19], [20], such as body walls [21]. A summary on representative numerical solvers for modeling nonlinear wave propagation in heterogeneous media is given below. Christopher and Parker [14] solved the equivalent Westervelt equation with an operator splitting method. The diffraction part was solved with the angular spectrum approach (ASA) and the nonlinearity term was solved by utilizing the frequency domain solution to Burgers' equation. This method is limited to parallel layered media [14]. Varslot and Taraldsen [22] derived a one-way model permitting smooth variation for all acoustical variables. A numerical solution to this equation was implemented using the operator splitting method. The Texas time-domain code was extended by Jing and Cleveland to solve the generalized Khokhlov-Zabolotskaya-Kuznetsov (KZK) equation and it is accurate for sound propagation in weakly heterogeneous media [23]. A modified ASA is developed [24] for media with spatially varying nonlinear parameter. A second-order wave equation describing nonlinear wave propagation in heterogeneous, attenuating media was solved with the finite-difference time-domain (FDTD) method by Pinton *et al.* [25]. A k-space time-domain method solving the coupled nonlinear wave equations was investigated [26] for modeling wave propagation in heterogeneous media with power law absorption. Almost at the same time, a k-space time-domain method for solving the second-order nonlinear wave equation was proposed [27] for thermoviscous fluids. Most recently, a mixed domain method (MDM) for modeling nonlinear one-wave propagation in dissipative, weakly heterogeneous media (speed of sound contrast being less than 1.1) has been presented [28]. A more detailed review on the modeling methods can be found in [29].

This work was supported by the U.S. National Institutes of Health under Grant R01EB025205. J. Gu was supported by a fellowship from the China Scholarship Council. *(Corresponding author: Yun Jing.)*

The authors are with the Department of Mechanical and Aerospace Engineering, North Carolina State University, Raleigh, NC 27695 UAS (e-mail: yjing2@ncsu.edu)

As demonstrated in [28], wave fields at a certain frequency can be produced by MDM in two ways for linear wave propagation. One is to obtain the result by applying the temporal Fourier transform to the transient simulation MDM result (denoted transient MDM, or TMDM). A more computationally efficient way is to directly implement the MDM at the frequency of interest (denoted frequency-specific MDM, or FSMDM). This carries a huge benefit especially when modeling continuous waves (CWs), which is often used in HIFU, since there is only a single frequency of interest and the latter approach could be orders of magnitude faster than the former. This benefit, however, is lost when modeling nonlinear wave propagation, since specific equations for describing harmonics are missing. In this paper, the FSMDM is extended to modeling the second harmonic ultrasound field in heterogeneous, lossy media for weakly nonlinear cases (Mach number $\varepsilon \ll 1$). First, the frequency-domain equation that describes the second harmonic frequency is derived. For weakly nonlinear cases, the fundamental frequency wave field is independent of the second harmonics, while the second harmonic wave field is directly produced by that of the fundamental frequency. To evaluate the accuracy of the FSMDM, four cases with imaginary tissue maps are investigated: wave propagation in a homogeneous nonlinear medium, a nonlinear medium with heterogeneous attenuation, a nonlinear medium with heterogeneous speed of sound, and a nonlinear medium with heterogeneous attenuation and speed of sound. Finally, a realistic human tissue map is used to evaluate the accuracy of the FSMDM. The FSMDM is compared with the TMDM throughout the paper.

II. Theory

The governing equation reads [28]

$$\nabla^2 p - \frac{1}{c^2}\frac{\partial^2 p}{\partial t^2} + \frac{\delta}{c^4}\frac{\partial^3 p}{\partial t^3} + \frac{\beta}{\rho c^4}\frac{\partial^2 p^2}{\partial t^2} = 0 \quad (1)$$

where p is the acoustic pressure, c is the speed of sound, t is the time, δ is the sound diffusivity and $\delta = 2\alpha c^3/\hat{\omega}^2$, where α is the absorption coefficient, $\hat{\omega}$ is the angular frequency, and β is the nonlinearity coefficient. All acoustical parameters vary spatially. The density is assumed to be a constant for simplification. For weakly nonlinear media, a quasilinear solution $p = p_1 + p_2$ is permitted [1], where p_1 is the pressure at the fundamental frequency ω and p_2 is the pressure at the second harmonic frequency 2ω. Additionally, it is assumed that $|p_1| \gg |p_2|$. By using the notation [1]

$$p_n(x,y,z,t) = \frac{1}{2i}P_n(x,y,z)e^{in\omega t} + c.c., \quad n = 1,2, \quad (2)$$

where $c.c.$ denotes the complex conjugate of preceding terms [1]. The pressure p can be expressed as

$$p(x,y,z,t) = \frac{1}{2i}P_1(x,y,z)e^{i\omega t} + \frac{1}{2i}P_2(x,y,z)e^{i2\omega t} + c.c. \quad (3)$$

For weakly nonlinear cases, we have the approximation

$$p^2(x,y,z,t) \cong -\frac{1}{4}P_1^2(x,y,z)e^{i2\omega t}. \quad (4)$$

Substituting (3) and (4) into (1) produces

$$\nabla^2\left(\frac{1}{2i}P_1 e^{i\omega t} + \frac{1}{2i}P_2 e^{i2\omega t}\right) - \frac{1}{c^2}\frac{\partial^2}{\partial t^2}\left(\frac{1}{2i}P_1 e^{i\omega t} + \frac{1}{2i}P_2 e^{i2\omega t}\right) = -\frac{\delta}{c^4}\frac{\partial^3}{\partial t^3}\left(\frac{1}{2i}P_1 e^{i\omega t} + \frac{1}{2i}P_2 e^{i2\omega t}\right) - \frac{\beta}{\rho c^4}\frac{\partial^2}{\partial t^2}\left(-\frac{1}{4}P_1^2 e^{i2\omega t}\right) \quad (5)$$

Rearranging (5) yields

$$\nabla^2 P_1 + \frac{\omega^2}{c^2}P_1 = \frac{i\omega^3\delta}{c^4}P_1 \quad (6)$$

and

$$\nabla^2 P_2 + \frac{4\omega^2}{c^2}P_2 = \frac{i8\omega^3\delta}{c^4}P_2 - \frac{i2\omega^2\beta}{\rho c^4}P_1^2 \quad (7)$$

Equation (6) should be solved first to calculate P_1. The fundamental frequency pressure will serve as part of the source term in (7) to calculate the second harmonic pressure P_2. Applying the Fourier transform to (6) and (7) with respect to x and y yields

$$\frac{\partial^2 \tilde{P}_1}{\partial z^2} + K_1^2\tilde{P}_1 = F_{xy}\left[\frac{i\omega^3\delta}{c^4}P_1 + \frac{\omega^2}{c_0^2}\left(1 - \frac{c_0^2}{c^2}\right)P_1\right] \quad (8)$$

and

$$\frac{\partial^2 \tilde{P}_2}{\partial z^2} + K_2^2\tilde{P}_2 = F_{xy}\left[\frac{i8\omega^3\delta}{c^4}P_2 + \frac{\omega^2}{c_0^2}\left(1 - \frac{c_0^2}{c^2}\right)P_2 - \frac{i2\omega^2\beta}{\rho c^4}P_1^2\right] \quad (9)$$

where $\tilde{P}_1(k_x, k_y, z)$ is the wave-vector domain pressure field at the fundamental frequency, $K_1^2 = \frac{\omega^2}{c_0^2} - k_x^2 - k_y^2$, where c_0 is a constant and is typically chosen as the minimum speed of sound in the medium under study, k_x and k_y are the wavenumbers in the x- and y-dimensions; $\tilde{P}_2(k_x, k_y, z)$ is the wave-vector domain pressure field at the second harmonic frequency, $K_2^2 = \frac{4\omega^2}{c_0^2} - k_x^2 - k_y^2$, where F_{xy} is the Fourier transform operator in the x- and y-dimensions. One-way propagation solutions to (8) and (9) can be found with the one-dimensional Greens function [28] and they are written as

$$\tilde{P}_1(z) = \tilde{P}_1(0)e^{iK_1 z} + \frac{e^{iK_1 z}}{2iK_1}\int_0^z e^{-iK_1 z'}\left\{F_{xy}\left[\frac{i\omega^3\delta}{c^4}P_1 + \frac{\omega^2}{c_0^2}\left(1 - \frac{c_0^2}{c^2}\right)P_1\right]\right\}dz' \quad (10)$$

and

$$\tilde{P}_2(z) = \tilde{P}_2(0)e^{iK_2 z} + \frac{e^{iK_2 z}}{2iK_2}\int_0^z e^{-iK_2 z'}\left\{F_{xy}\left[\frac{i8\omega^3\delta}{c^4}P_2 + \frac{\omega^2}{c_0^2}\left(1 - \frac{c_0^2}{c^2}\right)P_2 - \frac{i2\omega^2\beta}{\rho c^4}P_1^2\right]\right\}dz' \quad (11)$$

Equations (10) and (11) are solved with a Simpson-like scheme [28]. By applying the inverse Fourier transform to $\tilde{P}_1$ and $\tilde{P}_2$, the fundamental and second harmonic frequency pressure P_1 and P_2 can be obtained. This method, therefore, is denoted the FSMDM. Alternatively, the fundamental and second harmonic frequency wave fields can be obtained by applying the temporal Fourier transform to the transient simulation result. This is the TMDM and is described in [28].

III. Results

To validate the FSMDM, a case with three cylinders (two of them partially overlap) immersed in water is first studied and the corresponding acoustic medium is shown in Fig. 1(a). First, the cylinders are assumed to have the same acoustical properties as the water: speed of sound is 1500 m/s, density is 1000 kg/m^3, and nonlinearity coefficient is 3.6 for the whole domain. Source plane pressure amplitude is 1 MPa and the frequency is 1 MHz.

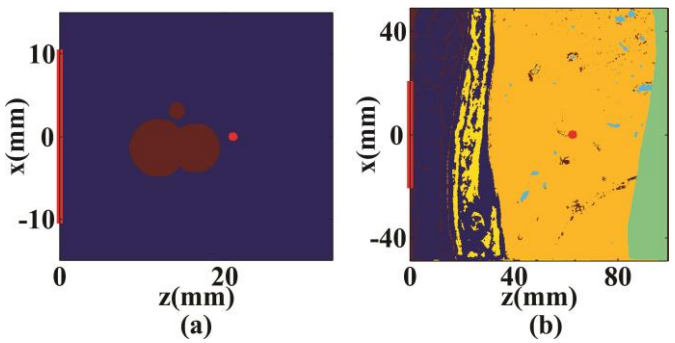

Fig. 1. (a) *In silico* model used for the first four cases where three cylinders having identical or different acoustical properties from the background medium are considered; (b) a realistic human tissue map with nonlinearity coefficient variation, speed of sound variation, and attenuation coefficient variation. The computational domain shown here are cropped form the original domain for illustration purposes. The superficial layer is connective tissue (red), then is fat (dark blue) with embedded connective tissue (red) and muscle (yellow), followed by liver (orange) and tissue (green). Blood (light blue) is inside the liver. The red line on the left boundary indicates the array position. The red dot is the geometrical focus.

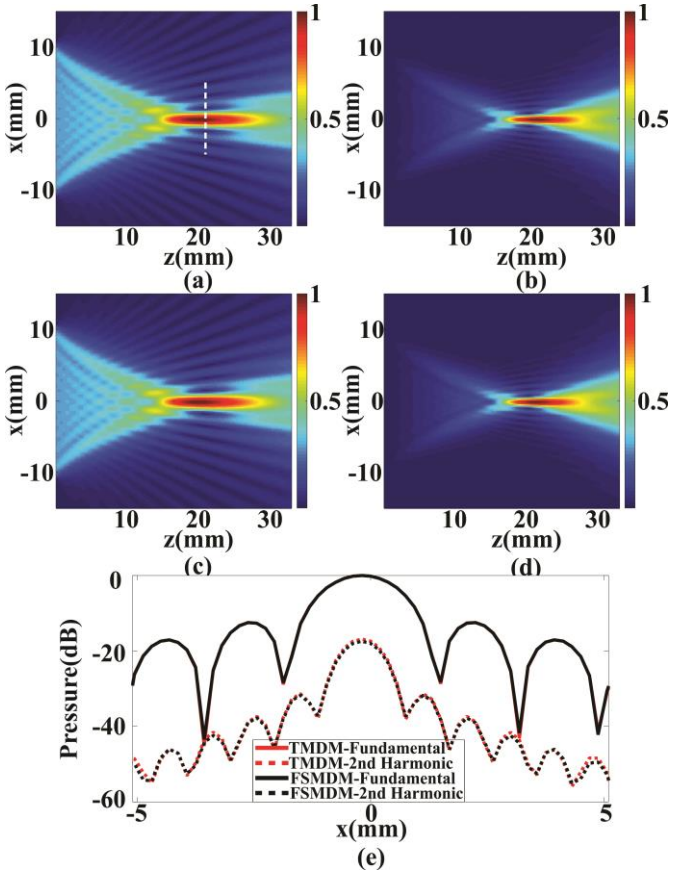

Fig. 2. Simulation results for the homogeneous medium case. (a) Fundamental frequency field and (b) the second harmonic field simulated by the TMDM. (c) Fundamental frequency field and (d) the second harmonic field simulated by the FSMDM. (e) Comparison for the pressure distribution along the white dashed line simulated by the TMDM and FSMDM.

A planar phased array is used to generate a focused ultrasound beam. Transducer diameter and focal length are both 14λ (λ is the wavelength in water and it is 1.5 mm). The transverse dimension of the computational domain is 100λ and the propagation distance is 22λ. The results from the TMDM are

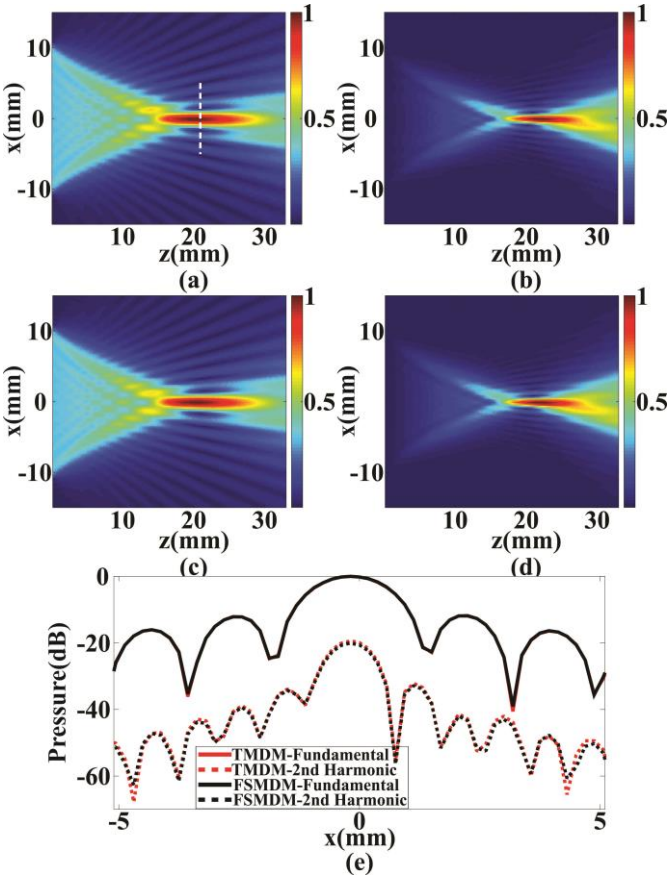

Fig. 3. Simulation results for the case with heterogeneous attenuation. (a) Fundamental frequency field and (b) the second harmonic field simulated by the TMDM. (c) Fundamental frequency field and (d) the second harmonic field simulated by the FSMDM. (e) Comparisons for the pressure distribution along the white dashed line simulated by the TMDM and FSMDM.

used as the benchmark and the accuracy of the TMDM has been confirmed in [28]. In the TMDM, a 40-cycle sine wave is applied as the input signal to mimic a continuous wave. For this and the next three cases involving cylinders, the spatial resolution in both the TMDM and FSMDM is 1/8λ and the temporal resolution in the TMDM is $1/(16f_c)$, where f_c is the fundamental frequency. The temporal domain size is 80 μs in the TMDM. L2 normalized errors are calculated to quantitatively analyze the accuracy of the FSMDM and they are defined as

$$L2 = \frac{\|p_{FSMDM} - p_{benchmark}\|}{\|p_{benchmark}\|}, \quad (12)$$

where $\|p\|$ is the L2 norm of the normalized acoustic pressure.

For the first case (homogeneous medium), the fundamental and second harmonic frequency pressure fields simulated by the TMDM and FSMDM are shown in Fig. 2. Figure 2(e) compares the fundamental and the second harmonic pressure distributions along the white dashed line (across the transducer geometrical focus). Pressures in Figs. 2(a)-(d) are normalized by the maximum pressure and pressures in Fig. 2(e) are normalized by the maximum fundamental frequency pressure. The agreement between the TMDM and FSMDM is very good. L2 norm errors are calculated with the normalized pressure for the focal region (a 16.5 mm by 3.0 mm rectangle centered around the focus) and they are 0.0044 for the fundamental frequency and 0.0112 for

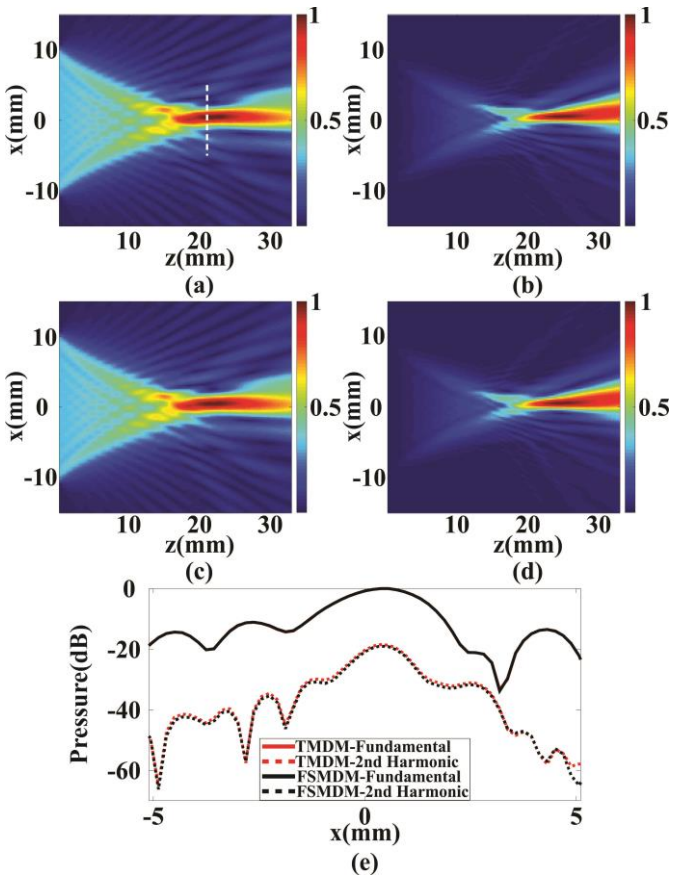

Fig. 4. Simulation results for the case with heterogeneous speed of sound. (a) Fundamental frequency field and (b) the second harmonic field simulated by the TMDM. (c) Fundamental frequency field and (d) the second harmonic field simulated by the FSMDM. (e) Comparisons for the pressure distribution along the white dashed line simulated by the TMDM and FSMDM.

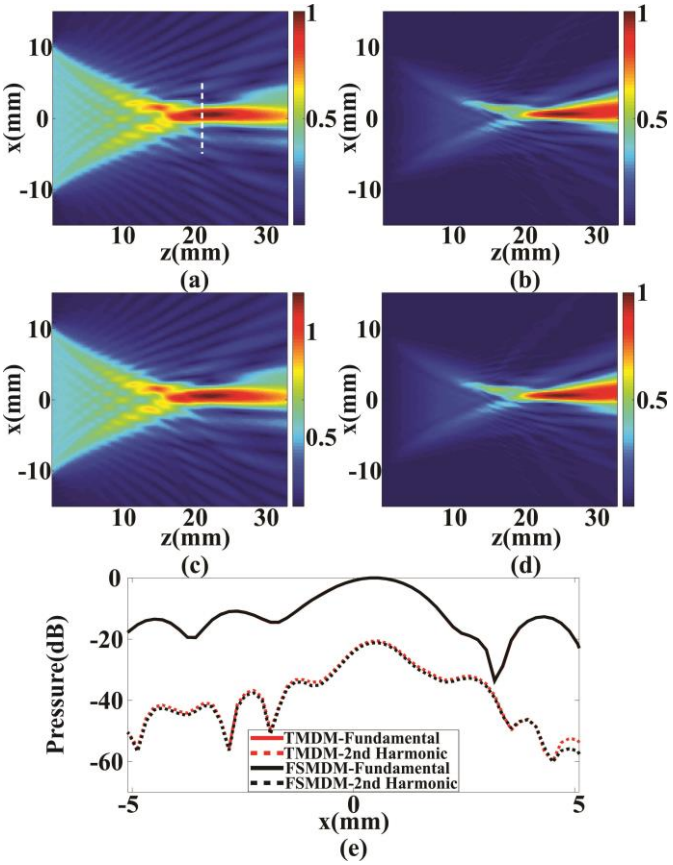

Fig. 5 Simulation results for the case with heterogeneous attenuation and speed of sound. (a) Fundamental frequency field and (b) the second harmonic field simulated by the TMDM. (c) Fundamental frequency field and (d) the second harmonic field simulated by the FSMDM. (e) Comparisons for the pressure distribution along the white dashed line simulated by the TMDM and FSMDM.

the second harmonics.

Next, heterogeneous attenuations are added to the nonlinear medium. The attenuation coefficient inside the cylinders is 1.5 dB·MHz^{-y}·cm^{-1} and is 0 outside the cylinders. The power law exponent y is equal to 2. Simulation results for the nonlinear medium with heterogeneous attenuations are plotted in Fig. 3. L2 norm errors (calculated for a 16.5 mm by 3.0 mm rectangle region centered around the focus) are 0.0039 for the fundamental frequency and 0.0107 for the second harmonics.

In the third case, the speed of sound variation is considered. The speed of sound inside the cylinders is 1575 m/s and is 1500 m/s outside the cylinders. Simulation results for this case are shown in Fig. 4. Defocusing is visible in this case due to phase aberration. Pressures are again normalized. L2 norm errors (calculated for a 16.5 mm by 4.3 mm rectangle centered around the focus) are 0.0046 for the fundamental frequency and 0.0145 for the second harmonics.

In the fourth case, both speed of sound variation and spatially varying attenuations are included. The attenuation coefficient inside the cylinders is 1.5 dB·MHz^{-y}·cm^{-1} and is 0 outside the cylinders. The power law exponent y is equal to 2. The speed of sound inside the cylinders is 1575 m/s and is 1500 m/s outside the cylinders. Normalized pressure fields simulated by the TMDM and FSMDM are illustrated and compared in Fig. 5. L2 norm errors (calculated for a 16.5 mm by 4.3 mm rectangle centered around the focus) are 0.0035 for the fundamental frequency and is 0.0119 for the second harmonics. Overall, these four cases exhibit similar levels of error.

To further validate the FSMDM, a realistic human tissue map with spatially varying speed of sound, attenuation, and nonlinearity is studied. The tissue map is illustrated in Fig. 1(b) and the acoustical properties for different tissue parts are listed in Table I [30]. The red line on the left boundary indicates the array position. The red dot is the geometrical focus. The temporal domain size in the TMDM is around 91 μs in this case. The spatial resolution is 0.165 mm and temporal resolution is $1/(16f_c)$. In this case, the fundamental frequency f_c is 0.7 MHz. The Kramers-Kronig dispersion relation is implemented by replacing the speed of sound c with c_p and $c_p = (1/\hat{c} + \alpha_0 \tan(\pi y/2)\hat{\omega}^{y-1})^{-1}$,where $\hat{c}$ is the sound speed at zero frequency [31], and the power law sound absorption follows $\alpha(\hat{\omega}) = \alpha_0 \hat{\omega}^y$, where α_0 is the absorption in Np·MHz^{-y}·m^{-1}. The fundamental and second harmonic frequency pressure fields simulated by the TMDM and FSMDM are shown in Figs. 6(a)-(e). Figure 6(e) compares the pressure distributions along the white dashed line (across the transducer geometrical focus). L2 norm errors (calculated for a 24.7 mm by 2.0 mm rectangle centered around the focus) are 0.0114 and 0.0185 for the

TABLE I
TISSUE ACOUSTICAL PROPERTIES

	Nonlin. Coef.	Speed of sound m/s	Density kg/m^3	Atten. Coef. @ 1 MHz (dB/cm)	Power law exponent *y*
connective	5.0	1613	1120	1.57	1.1
fat	5.8	1478	950	0.48	1.1
muscle	5.5	1547	1050	1.09	1.1
liver	4.3	1595	1060	0.5	1.2
blood	4.05	1584	1060	0.2	2.0
tissue	5.5	1540	1000	0.5	1.1

fundamental frequency and second harmonics, respectively.

IV. DISCUSSION

The FSMDM is an extension of the TMDM and is capable of modeling weakly nonlinear wave propagation in attenuating media with arbitrary, weak heterogeneities (in terms of the speed of sound [28]). Successive approximations have been made in deriving the equations for the fundamental frequency and second harmonics [1]. As a result, the fundamental frequency pressure is governed by the equation for linear acoustics. Using the quasilinear theory, the second harmonics can be solved by an equation where the fundamental frequency pressure is regarded as a source term on the right hand side of the equation. In this study, five cases, including a case using a realistic human tissue map, are used to evaluate the accuracy of the FSMDM. Results from the TMDM are used as the benchmark for calculating the errors. From the transverse pressure distribution comparison, it is shown that the FSMDM fundamental frequency pressures are almost identical to those of the TMDM for all cases. The L2 norm errors for the fundamental frequency field in the focal region are small and are on the order of 0.001 for the first four cases. This suggests that it is reasonable to assume that the fundamental frequency field is decoupled from those of harmonics at least for the cases under study, where the second harmonics amplitude is about 20 dB lower than that of the fundamental frequency. On the other hand, the FSMDM and TMDM also produce similar second harmonic ultrasound fields. For example, similar wave field distortions due to the presence of heterogeneities are observed. Though the L2 norm errors are larger when compared to the fundamental frequency, they are still reasonably small and are on the order of 0.01.

The numerical implementation throughout this study is based on MATLAB 2018a (The MathWorks Inc., Natick, MA) on a 64-bit operating system with a 12-core 3.00-GHz Intel Xeon (R) Gold 6136 CPU (Intel Corp., Santa Clara, CA) processor and 192 GB of RAM. Though TMDM and FSMDM show similar results for the same problem, the FSMDM is computationally superior. For example, to simulate the wave propagation using the human tissue map, the TMDM takes about 481.73 s while the FSMDM is two orders of magnitude faster, needing merely 2.82 s. This is because in the FSMDM, the pressure at the frequencies of interest can be directly obtained without running transient simulations.

The FSMDM suffers from several limitations and intrinsic errors though. The FSMDM uses the similar algorithm as that

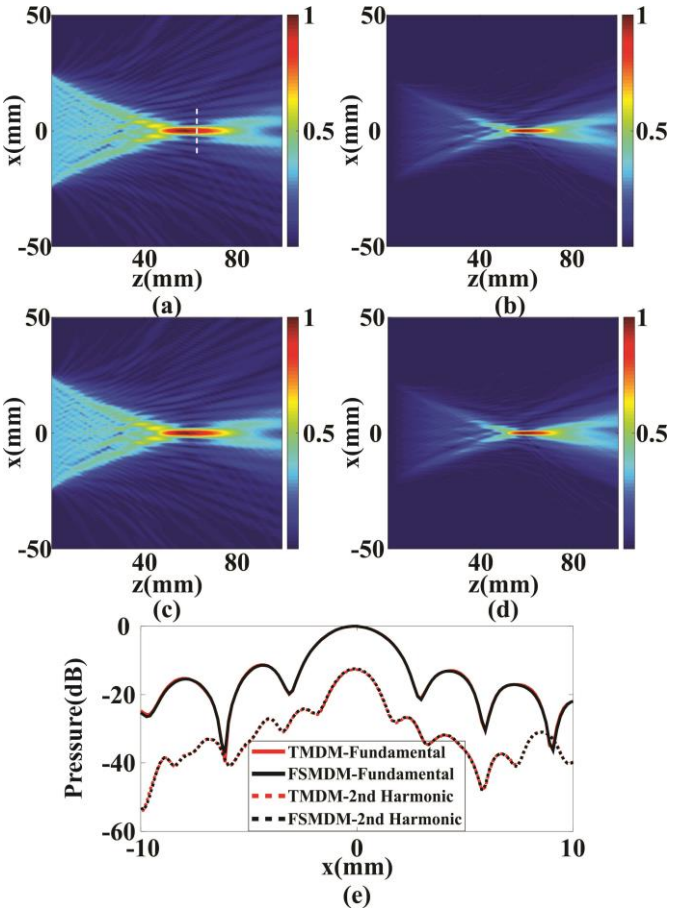

Fig. 6. Simulation results for the case of a realistic human tissue map. (a) Fundamental frequency field and (b) the second harmonic field simulated by the TMDM. (c) Fundamental frequency field and (d) the second harmonic field simulated by the FSMDM. (e) Comparisons for the pressure distribution along the white dashed line simulated by the TMDM and FSMDM.

of the TMDM [28], and the possible sources of errors should also be similar, and they are as follows: 1) the FSMDM is only accurate for media with weakly heterogeneous speed of sound, e.g., soft tissue; 2) the FSMDM is a one-way model and reflections are not included; 3) stair-casing errors [32] occur when representing complex geometries with rectilinear grids; 4) truncation errors introduced by numerical integration [33]; and 5) spatial aliasing errors [34] due to the finite-size computational domain. The spatial aliasing error is possibly more severe for the second harmonics. For most cases above, the L2 norm error for the fundamental frequency is considerably smaller than the second harmonics. This could be attributed to how the second harmonics are calculated in the FSMDM. The spatial aliasing error is first introduced to the fundamental frequency when implementing (10). This error is further carried into the second harmonic field, which contains its own spatial aliasing errors when implementing (11). To minimize this error, a larger domain should be considered. Alternatively, absorption layers can also be used to reduce the spatial aliasing error [35].

One limitation of the FSMDM is that the governing equations are derived with the quasilinear theory and they are only valid for weakly nonlinear cases [1], [24]. It would be interesting to examine when the quasilinear approximation would be

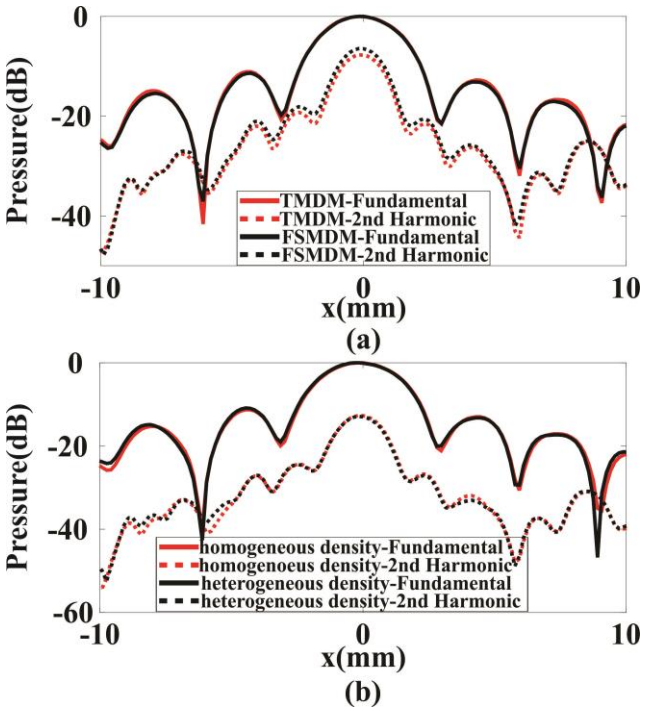

Fig. 7. (a) Comparison for the pressure distribution along the white dashed line (illustrated in Fig. 6(a)) simulated by the TMDM and FSMDM. (b) Comparison for the pressure distribution along the white dashed line (illustrated in Fig. 6(a)) simulated by the TMDM with and without density heterogeneities.

violated. To this end, pressure amplitude can be increased from 1 MPa to 2 MPa within the human tissue map. The transverse pressure distributions are show in Fig. 7(a) and the L2 norm errors for the same rectangle region are 0.0216 and 0.0559 for the fundamental frequency and second harmonics, respectively. As expected, the second harmonics calculated by the TMDM is much stronger than the previous case with 1 MPa pressure amplitude. It is now about 8 dB lower than the fundamental frequency. Since the quasilinear approximation fails in this case, the FSMDM is less accurate, indicated by the greater errors. It should also be pointed out that the FSMDM would overestimate the amplitude of the fundamental frequency, since it does not consider the energy transfer from the fundamental frequency to the second harmonics. Though only the second harmonics are studied here, governing equations for higher harmonics can also be derived [36]. Similarly, it is also possible to derive the equation for the difference frequency generated from the interaction of two fundamental frequencies, which is useful for studying problems such as nonlinear coefficient tomography and parametric arrays [1], [37]. All these equations can be subsequently solved by the FSMDM.

Finally, the FSMDM studied here does not consider density heterogeneities, though there is no fundamental barrier to do this. The simplification of considering homogeneous density is made based on the assumption that density heterogeneities have a less important role in affecting the acoustic field, particularly for soft tissue. Figure 7(b) compares the transverse pressure distribution in the human tissue map with and without density heterogeneities using the TMDM. Density values for the tissue map are listed in Table I. Using the results with density heterogeneities as the benchmark, the L2 norm errors in the same focal region are 0.0311 and 0.0287 for the fundamental frequency and second harmonics, respectively. These results suggest that the density variation does not significantly affect the acoustic field in soft tissue and can be neglected.

V. Conclusion

The FSMDM is presented and evaluated in this study for the simulation of the second harmonic ultrasound field. The governing equation for the second harmonic is derived using the quasilinear theory. Attenuation, speed of sound, and nonlinear coefficient are all spatially varying functions. The FSMDM is introduced to solve the governing equation for the second harmonics. Five various cases are investigated to validate the FSMDM for weakly nonlinear and weakly heterogeneous media. Simulation results show that the FSMDM and its counterpart (TMDM) give similar results for all five cases. However, the computational speed of the FSMDM is substantially faster than the TMDM. Due to this advantage, the FSMDM could be proven useful for a variety of applications such as HIFU treatment planning and nonlinearity coefficient tomography.

Acknowledgment

The authors would like to thank Dr. Gianmarco Pinton for providing the human tissue map.

References

[1] M. F. Hamilton and D. T. Blackstock, Nonlinear acoustics, San Diego: Academic press, 1998.
[2] B. Ward, A. Baker, and V. Humphrey, "Nonlinear propagation applied to the improvement of resolution in diagnostic medical ultrasound," *J. Acoust. Soc. Am.*, vol. 101, pp. 143-154, 1997.
[3] F. Tranquart, N. Grenier, V. Eder, and L. Pourcelot, "Clinical use of ultrasound tissue harmonic imaging," *Ultrasound med. biol.*, vol. 25, pp. 889-894, 1999.
[4] D. Zhang, X. Chen, and X.-f. Gong, "Acoustic nonlinearity parameter tomography for biological tissues via parametric array from a circular piston source—Theoretical analysis and computer simulations," *J. Acoust. Soc. Am.*, vol. 109, pp. 1219-1225, 2001.
[5] A. Cai, J.-a. Sun, and G. Wade, "Imaging the acoustic nonlinear parameter with diffraction tomography," *IEEE Trans. Ultrason., Ferroelectr., Freq. Control*, vol. 39, pp. 708-715, 1992.
[6] P. B. Rosnitskiy, P. V. Yuldashev, O. A. Sapozhnikov, A. D. Maxwell, W. Kreider, M. R. Bailey, et al., "Design of HIFU transducers for generating specified nonlinear ultrasound fields," *IEEE Trans. Ultrason., Ferroelectr., Freq. Control*, vol. 64, pp. 374-390, 2017.
[7] G. Pinton, J. F. Aubry, M. Fink, and M. Tanter, "Effects of nonlinear ultrasound propagation on high intensity brain therapy," *Med. phys.*, vol. 38, pp. 1207-1216, 2011.
[8] K. Hynynen, "The role of nonlinear ultrasound propagation during hyperthermia treatments," *Med. phys.*, vol. 18, pp. 1156-1163, 1991.
[9] K. Hynynen, "Demonstration of enhanced temperature elevation due to nonlinear propagation of focussed ultrasound in dog's thigh in vivo," Ultrasound in Medicine and Biology, vol. 13, pp. 85-91, 1987.
[10] W. Swindell, "A theoretical study of nonlinear effects with focused ultrasound in tissues: an “Acoustic Bragg Peak”," *Ultrasound med. biol.*, vol. 11, pp. 121-130, 1985.
[11] P. V. Yuldashev, S. M. Shmeleva, S. A. Ilyin, O. A. Sapozhnikov, L. R. Gavrilov, and V. A. Khokhlova, "The role of acoustic nonlinearity in tissue heating behind a rib cage using a high-intensity focused ultrasound phased array," *Ultrasound med. biol.*, vol. 58, p. 2537, 2013.
[12] X. Zhang, G. E. Owens, H. S. Gurm, Y. Ding, C. A. Cain, and Z. Xu, "Noninvasive thrombolysis using histotripsy beyond the intrinsic

threshold (microtripsy)," *IEEE Trans. Ultrason., Ferroelectr., Freq. Control*, vol. 62, pp. 1342-1355, 2015.

[13] M. S. Canney, V. A. Khokhlova, O. V. Bessonova, M. R. Bailey, and L. A. Crum, "Shock-induced heating and millisecond boiling in gels and tissue due to high intensity focused ultrasound," *Ultrasound med. biol.*, vol. 36, pp. 250-267, 2010.

[14] P. T. Christopher and K. J. Parker, "New approaches to nonlinear diffractive field propagation," *J. Acoust. Soc. Am.*, vol. 90, pp. 488-499, 1991.

[15] J. Tavakkoli, D. Cathignol, R. Souchon, and O. A. Sapozhnikov, "Modeling of pulsed finite-amplitude focused sound beams in time domain," *J. Acoust. Soc. Am.*, vol. 104, pp. 2061-2072, 1998.

[16] R. J. Zemp, J. Tavakkoli, and R. S. Cobbold, "Modeling of nonlinear ultrasound propagation in tissue from array transducers," *J. Acoust. Soc. Am.*, vol. 113, pp. 139-152, 2003.

[17] Y. Jing, M. Tao, and G. T. Clement, "Evaluation of a wave-vector-frequency-domain method for nonlinear wave propagation," *J. Acoust. Soc. Am.*, vol. 129, pp. 32-46, 2011.

[18] I. M. Hallaj and R. O. Cleveland, "FDTD simulation of finite-amplitude pressure and temperature fields for biomedical ultrasound," *J. Acoust. Soc. Am.*, vol. 105, pp. L7-L12, 1999.

[19] G. F. Pinton, G. E. Trahey, and J. J. Dahl, "Sources of image degradation in fundamental and harmonic ultrasound imaging using nonlinear, full-wave simulations," *IEEE Trans. Ultrason., Ferroelectr., Freq. Control*, vol. 58, 2011.

[20] T. Varslot, S.-E. Masoy, T. F. Johansen, and B. Angelsen, "Aberration in nonlinear acoustic wave propagation," *IEEE Trans. Ultrason., Ferroelectr., Freq. Control*, vol. 54, 2007.

[21] X. Yan and M. F. Hamilton, "Angular spectrum decomposition analysis of second harmonic ultrasound propagation and its relation to tissue harmonic imaging,", in *Ultrasonic and Advanced Methods for Nondestructive Testing and Material Characterization*, N. Dartmouth, MA, 2007, pp. 155-168.

[22] T. Varslot and G. Taraldsen, "Computer simulation of forward wave propagation in soft tissue," *IEEE Trans. Ultrason., Ferroelectr.*, vol. 52, pp. 1473-1482, 2005.

[23] Y. Jing and R. O. Cleveland, "Modeling the propagation of nonlinear three-dimensional acoustic beams in inhomogeneous media," *J. Acoust. Soc. Am.*, vol. 122, pp. 1352-1364, 2007.

[24] F. Varray, A. Ramalli, C. Cachard, P. Tortoli, and O. Basset, "Fundamental and second-harmonic ultrasound field computation of inhomogeneous nonlinear medium with a generalized angular spectrum method," *IEEE Trans. Ultrason., Ferroelectr.*, vol. 58, 2011.

[25] G. F. Pinton, J. Dahl, S. Rosenzweig, and G. E. Trahey, "A heterogeneous nonlinear attenuating full-wave model of ultrasound," *IEEE Trans. Ultrason., Ferroelectr.*, vol. 56, 2009.

[26] B. E. Treeby, J. Jaros, A. P. Rendell, and B. Cox, "Modeling nonlinear ultrasound propagation in heterogeneous media with power law absorption using a k-space pseudospectral method," *J. Acoust. Soc. Am.*, vol. 131, pp. 4324-4336, 2012.

[27] Y. Jing, T. Wang, and G. T. Clement, "A k-space method for moderately nonlinear wave propagation," *IEEE Trans. Ultrason., Ferroelectr.*, vol. 59, pp. 1664-1673, 2012.

[28] J. Gu and Y. Jing, "Numerical Modeling of Ultrasound Propagation in Weakly Heterogeneous Media Using a Mixed Domain Method," *IEEE Trans. Ultrason., Ferroelectr.*, vol. 65, pp. 1258-1267, 2018.

[29] J. Gu and Y. Jing, "Modeling of wave propagation for medical ultrasound: a review," *IEEE Trans. Ultrason., Ferroelectr.*, vol. 62, pp. 1979-1992, 2015.

[30] T. D. Mast, "Empirical relationships between acoustic parameters in human soft tissues*," Acoust. Res. Lett. Online*, vol. 1, no. 2, pp. 37–42, 2000

[31] T.L. Szabo, " Causal theories and data for acoustic attenuation obeying a frequency power law," *J. Acoust. Soc. Amer.*, vol. 97, no. 1, pp. 14–24, 1995.

[32] J. L. Robertson, B. T. Cox, J. Jaros, and B. E. Treeby, "Accurate simulation of transcranial ultrasound propagation for ultrasonic neuro-modulation and stimulation," *J. Acoust. Soc. Am.*, vol. 141, no. 3, pp. 1726–1738, 2017.

[33] D. L. Phillips, "A technique for the numerical solution of certain integral equations of the first kind," *J. ACM*, vol. 9, no. 1, pp. 84–97, 1962.

[34] P. Wu, R. Kazys, and T. Stepinski, "Analysis of the numerically implemented angular spectrum approach based on the evaluation of two - dimensional acoustic fields. Part I. Errors due to the discrete Fourier transform and discretization," *J. Acoust. Soc. Am.*, vol. 99, pp. 1339-1348, 1996.

[35] Y. Jing, "On the use of an absorption layer for the angular spectrum approach (L)," *J. Acoust. Soc. Am.*, vol. 131, pp. 999-1002, 2012.

[36] M. Pasovic, M. Danilouchkine, A. Van Der Steen, O. Basset, N. De Jong, and C. Cachard, "Extended angular spectrum method for calculation of higher harmonics," in *10ème Congrès Français d'Acoustique*, Lyon, France, 2010.

[37] W.-S. Gan, J. Yang, and T. Kamakura, "A review of parametric acoustic array in air," *Appl. Acoust.*, vol. 73, pp. 1211-1219, 2012.